

INSTITUTO SUPERIOR TÉCNICO

MSC BIOMEDICAL ENGINEERING

# Hard Tissue Project

## Tissue Biomechanics

André Faria n° 73569  
Sofia Monteiro n° 76827

FACULTY  
João Folgado  
Fernando Simões

May 23, 2016

---

### Abstract

Hip resurfacing is a minimally invasive hip replacement implant, allowing for the preservation of most of the epiphysis. The potential issues leading to failure of this type of prostheses include dislocations and femoral neck fracture, thus the changes of bone density distribution in specific locations is of concern. In order to estimate bone remodelling following the placement of a Cobalt-Chromium hip resurfacing implant, a finite element method analysis, using a fourth order Runge-Kutta's iterative method, with ABAQUS was implemented, along with the Huiskes Model programmed in MATLAB. For this bone model, a  $k$  value of 0.00275 J/g was the one that better reproduced the density distribution across the proximal femur. No significant differences were observed with the introduction of plateaus (with  $s$  values of 9, 20 and 40%). Several alterations in hip resurfacing design were studied. The differences in bone remodelling with stem sizes of 25, 50 and 75 mm were significant. No meaningful distinctions were found when using an isoelastic (*i.e.*, E=17GPa) stem in alternative to a Co-Cr (*i.e.*, E=130GPa) stem.

## 1 Introduction

Orthopaedic implants are the second most frequent implants<sup>1</sup>. Over decades, the approach to implant design has evolved extensively, with different directions. One of the current concerns is to reconsider the balance and harmony between mechanics and biology, the tendency being to make an effort in order not to sacrifice the physiological native functions. One way to achieve this is to preserve as much healthy native tissue as possible. Hip resurfacing is a type of total hip replacement that attempts to meet this goal. Its benefits are especially appealing for young patients, reducing the concerns with the possibility of revision surgery. This type of prosthesis is not, however, free of controversy regarding the drawbacks of this procedure. The risks associated result in a higher failure rate than standard total hip replacement.

The use of the finite element method with the software ABAQUS and the application of a bone remodelling model with MATLAB allow for a study of some of the potential risks associated with Cobalt Chromium hip resurfacing. In this project, we shall investigate the impact of Cobalt Chromium hip resurfacing on bone density in the proximal femur and infer about the potential for

---

<sup>1</sup>Dental implants are preformed the most.

femoral neck fracture. In the resurfaced bone, besides the formation of a physiological medullary cavity with null density, we predict bone loss (*i.e.*, reduction of density) on the sides of the stem due to stress shielding, as well as reinforcement of the bone distally to the stem end.

## 2 Physiological and Anatomical Context

### 2.1 Bone

Besides accounting for synthetic and metabolic functions, such as blood cell production and nutrient store, bone has a major structural purpose in the human organism as the primary tissue composing the skeleton. Bone is responsible for withstanding impact and protecting internal organs. Tendons attach to bone, allowing the muscles to act on the joints and induce movement. Its mechanical properties reflect the load carrying functions through great stiffness and toughness. After enamel and dentin, cortical bone is the hardest tissue in the human body (*i.e.*, with highest Young's Modulus) [1].

As most tissues, bone is composed of both cells and extracellular matrix ECM. The ECM of bone has a mineral and an organic phase. The mineral phase of bone is essentially hydroxyapatite CaP (a calcium and phosphate apatite), whose crystals have a fusiform shape and are dispersed in alignment with collagen fibers. The mineral provides stiffness to the bone<sup>2</sup>, while toughness and work of fracture are regulated by the organic phase.

Component	Amount (w/o)
Mineral (apatite)	69
Organic matrix	22
collagen	(90–96% of organic matrix)
others	(4–10% of organic matrix)
Water	9

Figure 1: Composition of Bone

Despite its robustness, adult bone may physiologically readjust its internal features in order to optimize the mechanical properties in response to a change in mechanical stimuli. This structural adaptation of bone to activity and function is known as bone remodelling.

#### 2.1.1 Bone Structure

The structure of bone can be described as a series of bone surfaces, one of which is the Haversian canal. In both primary and secondary bone, the first level structure is composed of Haversian systems or osteons, with diameter between 200 and 300 micrometers. Concentric lamellae of collagen fiber sheets form each one of the osteons, which – in long bones – are mostly parallel to the long axis of the diaphysis (*see* Figure 2). This leads to an anisotropic behavior, with the longitudinal direction having Young's modulus, compressive and tensile strengths 2 times greater than in the radial direction and 1.5 than the tangential direction [1].

The collagen fibers are parallel to each other within lamellae and may have different orientations between lamellae. In the center of the system, the Haversian canal is occupied by vessels, which account for the supply of oxygen and nutrients and depletion of metabolites of the highly active metabolism of bone tissue [2]. The above structure corresponds to cortical bone, whereas

---

<sup>2</sup>A higher mineral content and consequent higher density leads to a higher Young's modulus.

in trabecular bone trabecula replace osteons. Cortical bone has greater stiffness and trabecular bone accounts for ductility.

The orientation of the internal structures of bone depends on the specific loads applied on the bone. Wolff's law states that bone remodelling is favored in a way that leads to the alignment of both the mineral and organic phases along the principal stress trajectories, as seen in Figure 3. Biologically, this requires that the synthesis of matrix and mineral deposition are greater at regions of larger mechanical stress, and bone resorption increases in regions of smaller stress. As a consequence, the morphology of bone is determined by its function.

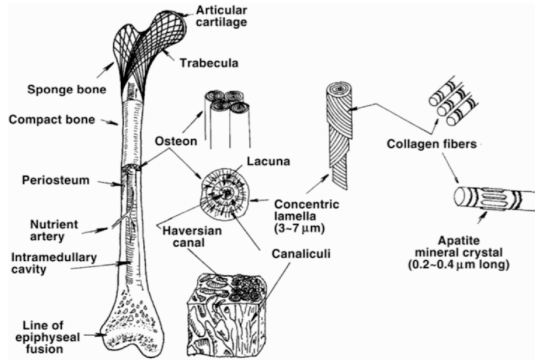


Figure 2: Organization of a typical bone.

### 2.1.2 Bone Remodeling

Once the loads applied to the bone are determined, a harder biomechanical problem follows: to predict the long term effects of these loads. For that, the concepts of local stress, strain and energy are essential. Although bone is considered a hard tissue, it is slightly deformable in physiological situations. Small local deformations might be responsible for the changes in local structure and density under a certain load. If the density distribution (*i.e.*, bone quantity) is altered, then so is the mechanical response of the bone to the same load (*e.g.*, if, after remodelling, the density and elastic modulus increase, the same load may lead to less deformation) [1].

Bone remodelling is a continuous process in human bone, regulated by the balance between osteoblast and osteoclast activity, as well as nutrient and ion (*e.g.*, Calcium) supply, and is macroscopically depicted as the more popular formulation of Wolff's Law, which states that bone is reshaped due to the forces acting on it [2]. The biological mechanisms of strain field sensing and the feedback systems that regulate bone remodelling at the cellular lever are still not fully understood. However, there are mathematical models that characterize the changes in bone density in response to the mechanical phenomena occurring locally inside the bone [3]. In this project, we adopt the Huskies bone remodelling model (*see* Section 4.1), in order to predict the bone density changes triggered by different types of loads on both normal bone and bone with a hip resurfacing prosthesis.

## 2.2 Hip Joint

### 2.2.1 Femur

In this project we consider the superior portion of a femur (*i.e.*, proximal femur), a long bone which is the heaviest, lengthiest and most resistant bone in the human body. In its proximal

end, the femoral head is inserted in the acetabulum, assembling the hip joint. The femoral neck, which follows the head laterally, is a common area of bone fracture. On the other side of the superior epiphysis is the greater trochanter, where several muscles have insertions [4][5]. The distal epiphysis is not considered in our model (*see* Section 3).

The external part of the femur is composed of cortical bone, surrounding the trabecular bone. As in all long bones, there is a central cavity along the main axis of the femur that houses the bone marrow, responsible for hematopoiesis. Our initial model (*see* Section 3) assumes uniform density, but we expect it to acquire the density features described above by iteratively applying a bone remodelling model, under loads similar to the physiological ones.

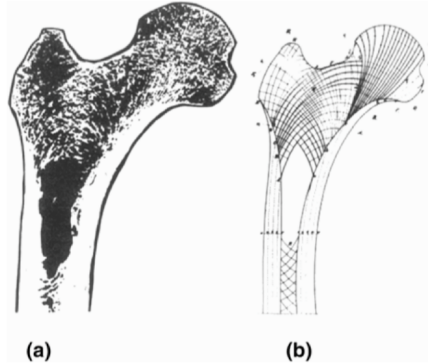


Figure 3: (a) Frontal section of the proximal femur; (b) orientation of the bone matrix structure

### 2.2.2 Loading

We are concerned with the loads applied to the femur via the hip joint and the muscles responsible for abduction (*i.e.*, the movement of drawing the leg outwards in the coronal plane). Joints are major points of force transfer in the skeleton and the hip joint is the most loaded and stable enarthrosis (*i.e.*, ball and socket joint) in the human body. We will investigate the bone remodelling response to a combination of two loading situations, the walking and stair climbing movements, in the normal bone and also in the case of hip resurfacing.

In reality, the movements studied are cyclic, involving a swing phase and a stance phase for each of the lower limbs. During a portion of the gait cycle<sup>3</sup>, only one foot is in contact with the ground and a single leg bears the whole body weight<sup>4</sup>. The stair climbing movement involves loads that can go up to five times the body weight [6].

The loads considered in our modulation correspond to a two dimensional static analysis of this portion of the movement, when the forces have the greatest intensity<sup>5</sup>. Each loading case involves two forces on the femur: a compressive force is applied in the femoral head, corresponding to the joint reaction force at the point of interaction with the middle of the acetabulum; a tensile force from the medium and minimum gluteal muscles (*i.e.*, hip abductors) is applied at their point of insertion in the greater trochanter [5] [7].

<sup>3</sup>More precisely, during the last two thirds of the stance phase

<sup>4</sup>About five sixths of the body weight

<sup>5</sup>This choice of loads is not necessarily the most appropriate, since the highest loads are not necessarily the most damaging ones

### 2.2.3 Hip Resurfacing

The most prevalent joint pathology is arthritis; it is also the most common reason for hip replacement. Arthritis damages the cartilage and, further on, the bone. Implants are placed in case of severe compromise of the tissue, whose purpose is to replace the normal functional and structural features of the native joint. One million total joint replacement procedures are performed in the US yearly; hip replacement accounts for about a third of those.

Hip resurfacing is an alternative to the standard arthroplasty procedure, total hip replacement (THR), which involves the removal of a significant portion of bone and its subsequent replacement with a synthetic prosthesis. Most pathological situations leading to the placement of hip prostheses involve only local damage to tissue around the joint. Nevertheless, a substantial amount of healthy bone is sacrificed in THR<sup>6</sup>. Hip resurfacing provides a minimally invasive alternative to THR, which is particularly appealing for young patients who have a significant chance of needing revision surgery in the long term.

Although hip resurfacing has a higher long term failure risk at eight years, it has the advantage of sparing the native tissues, involving only the removal of a minimal volume of both the femur and the acetabulum<sup>7</sup>. Since the cups have a reduced thickness (*see* Figure 7), all-metal components are preferred (rather than polymer-metal or ceramic-metal, which are common in THR), so they belong to the category of metal-on-metal prostheses [8].

The surfaces and stems are made of Cobalt Chromium alloys: due to their hardness they are more resistant to wear and therefore are more suitable for the head components of prostheses. However, the high elastic modulus comes at the expense of significant stress shielding. Having a much high elastic modulus than the bone, the prosthesis bears greater stress. As such, the distribution of stresses in the prosthesis and bone is not uniform and the stress transmitted to the bone is lowered (relative to intact bone) leading to bone resorption. Titanium alloys are usually preferred in the stems of classical implants, since their hardness is closer to the one of bone and therefore reduce the resorption due to shielding. Titanium also accounts for better bio-compatibility features<sup>8</sup>. However, mixing two different metals in a single implant is undesirable because it leads to establishment of an electrochemical cell that eventually causes galvanic corrosion.

One of the potential complications arising from hip resurfacing procedures is femoral neck fracture, which is consistent with the expectation of stress shielding around the stem. This and other concerns related to the high failure rate of hip resurfacing have made it globally unpopular. The FDA<sup>9</sup> has enforced recalls on most devices in the market, and currently approves only a very limited number of them.

## 3 Problem Formulation

As mentioned above, the bone remodelling response is to be determined in several cases. We consider a combination of two loading profiles, walking and stair climbing, for both the intact femur and the femur with a non-cemented hip resurfacing prosthesis. We tested a full Co-Cr prosthesis, a prosthesis with a iso-elastic stem and also three stem sizes. The material properties and the forces considered are presented in Figure 4.

---

<sup>6</sup>This becomes troublesome when there is the need for revision surgery, which is frequently needed due to failure, since removing bone compromises the sustainability of the femur for future procedures.

<sup>7</sup>Furthermore, it has been argued that the preservation of the dimensions of the head and acetabulum reduces the risk of dislocations and improves joint lubrication.

<sup>8</sup>Cromium and Nickel, which are present in Co-Cr alloys, may cause allergic reactions in about 7% of the population

<sup>9</sup>Food and Drug Administration

According to the adoption of a two dimensional formulation of the Huiskes Model (see Section 4.1), we consider that the bone is an isotropic material. At the starting point, the bone is homogeneous (*i.e.*, uniform density and elastic modulus throughout the body) with elastic modulus equal to the one of cortical bone. Then, for each case, the density distribution across the given bone section after remodelling is determined. The final purpose is to study the bone adaptation that follows a hip resurfacing procedure.

Propriedades dos materiais			
		E (GPa)	v
Osso	Tecido ósseo (osso compacto)	17	0.3
Haste	Co-Cr / Iso-elástico* (caso académico)	130 / 17	0.3

Forças aplicadas			
Caso de carga	F <sub>x</sub> (N)	F <sub>y</sub> (N)	F <sub>z</sub> (N)
F <sub>h</sub>	-224	-2246	-972
F <sub>a</sub>	768	1210	726
F <sub>h</sub>	457	-1707	-769
F <sub>a</sub>	383	547	669

Figure 4: Material Properties and Loads

## 4 Methods

### 4.1 Huiskes Model

There are several mathematical models that quantitatively depict bone adaptation. They describe the variation in bone density as a function of mechanical stimuli. In this project we consider the Huiskes model, which considers bone as isotopic and uses the strain energy density  $U$  as the relevant stimulus for determining the velocity of bone adaptation  $d\rho/dt$ .  $U$  is given by:

$$U = \frac{1}{2} \sigma_{ij} \epsilon_{ij} \quad (1)$$

Under the assumptions of this model, the mathematical relationship for internal bone adaptation<sup>10</sup> is given by:

$$\frac{d\rho}{dt} = \begin{cases} B\left(\frac{U}{\rho} - k(1-s)\right), & \text{if } \frac{U}{\rho} < k(1-s) \\ 0, & \text{otherwise} \\ B\left(\frac{U}{\rho} - k(1+s)\right), & \text{if } \frac{U}{\rho} > k(1+s) \end{cases} \quad (2)$$

where  $\rho$  is the apparent density,  $t$  is the time variable,  $B$  is a parameter and  $s$  corresponds to half of the length of the plateau in which there is no stimulus to bone adaptation (*i.e.*, the range of strain energy densities for which  $d\rho/dt$  is zero). Finally,  $k$  corresponds to the average strain energy density (*i.e.*, the value of  $U/\rho$  at the middle of the plateau). The reference values  $s$  and  $k$  should ideally be adapted to the situation being studied [9]. The first branch of equation 2

---

<sup>10</sup>Since we consider the outside shape of the bone to be constant, there is no external adaptation.

corresponds to bone loss (*i.e.*, bone resorption) while the third branch is due to bone formation (*i.e.*, synthesis and mineralization).

The width of the so called "lazy zone" (*i.e.*, the plateau), depicted in Figure 5, reflects the sensitivity of the bone to stimuli. Therefore, a larger plateau means the bone needs a greater deformation energy to trigger adaptation. Young bone will readily remodel under a small stimulus, whereas mature bone will require greater strain deformations for the same remodelling. As such, higher values of  $s$  generally correspond to older bones.

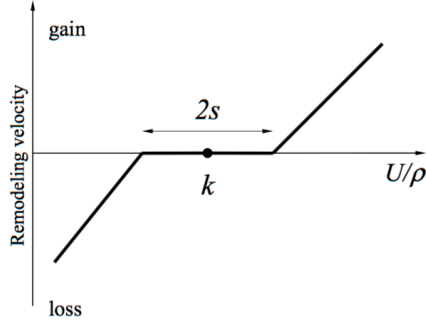


Figure 5: Graphical representation of Huiskes Model. The plateau with width  $2s$  and center in  $k$  is the region of null stimulus for bone remodeling. [3]

In the limiting case in which there is no "lazy zone" (*i.e.*,  $s = 0$ ), the Huiskes Model is simplified to:

$$\frac{d\rho}{dt} = B \left( \frac{U}{\rho} - k \right) \quad (3)$$

The Young's modulus  $E$  of bone, which is needed for the Finite Element Method implementation, is a function of bone density:

$$E = 3790\rho^3 \quad (4)$$

where  $\rho$  is usually in a range from 0.01 to  $1.74 \text{ g/cm}^3$  [3].

The rationale for the parameter choice and the methods used in the computational implementation are presented in Sections 5.2.1 through 5.2.4.

## 4.2 Finite Element Method

The finite element method FEM is a numerical method for solving differential equations. It has become popular in diverse engineering applications since the evolution of computers allowed the implementation of computationally demanding routines [10]. The FEM yields an approximate solution to a problem which could not be practically solved with analytical methods [11].

In this method, the domain of the problem (*i.e.*, the structure being studied) is discretized into simpler and non intersecting subdomains, called elements, which can have a variety of geometric shapes. In each element there are several nodes, which along with their interconnections form the mesh. Approximating functions (usually polynomial functions) are defined for each element, and the elements are assembled in order to ensure continuity, force balance and the border constraints.

The FEM involves determining the weak formulation of the differential equation that models the problem, requiring for that the Virtual Power Principle VPP, which derives from energy conservation, and is given by:

$$\int_{\Omega} \sigma_{ij} \bar{\epsilon}_{ij} d\Omega = \int_{\Omega} X_{ij} \bar{u}_{ij} d\Omega + \int_{\Gamma} t_{ij} \bar{u}_{ij} d\Gamma + \quad (5)$$

Taking into account the properties of hard tissue, we simplified the problem as one of linear elasticity. In this case, the constitutive law relates stresses and deformations in the body and is known as generalized Hooke's Law [12]:

$$\sigma_{ij,j} = E_{ijkl} \epsilon_{kl} \quad (6)$$

The combination of the VPP, which is valid under any constitutive law, and the generalized Hooke's Law yields, for this problem:

$$\int_{\Omega} E_{ijkl} \epsilon_{kl}(u) \bar{\epsilon}_{ij}(w) d\Omega = \int_{\Omega} X_{ij} \bar{w}_{ij} d\Omega + \int_{\Gamma} t_{ij} \bar{w}_{ij} d\Gamma + \quad (7)$$

### 4.3 Two Dimensional Model and Side Plate

Our problem will be simplified in a two dimensional model of the femur (from now on referred to as 2D model). The two dimensional approach leads to a significant reduction of the computational burden of this analysis, but largely ignores some of the mechanical features of real bone. For example, both Huiskes and 2D models fail to adequately embed the anisotropic behavior of the bone (*i.e.*, the variations of mechanical properties according to the three main directions) (*see* Section 2.1.1) Another simplification is the initial assumption of the cortical bone Young's modulus for the whole structure. A side plate is introduced in order to preserve a key aspect of the three dimensional mechanical properties of bone, while maintaining the easiness of a two dimensional analysis.

The need for a side plate results from the following issue: as the medullary cavity is formed, the two lateral sides of the bone become disconnected in the two dimensional model; then the bone stops behaving as a single beam, which leads to the establishment of oblique structures inside the canal that re-connect both sides. By using a side plate [13], forces are transmitted from one side of the cavity to the other, so the bone can behave as a single beam without sacrificing the medullary cavity: this greatly improves the planar simulation the three dimensional hollow cylindrical character of the bone<sup>11</sup>.

## 5 Computational Implementation

### 5.1 Proximal Femur Modelling in Abaqus

In this section, we outline the most relevant steps of the two dimensional proximal femur modelling in ABAQUS.

The drawings of the several parts - bone, side plate, cut bone and prosthesis - were done according to the sketches in Figures 6 and 7.

The side plate was divided into three sections - superior, medial and inferior - each one with its own thickness - 1, 3 and 5 mm respectively.

---

<sup>11</sup>The same problem happens with the insertion of the prosthesis in the 2D model: proximal regions on opposite sides of the stem become disconnected. In real bone, however, there is bone surrounding the stem and thus there is transfer of stress between the bone on the two sides. Again, in this case the side plate allows the loads to pass from one side to the other

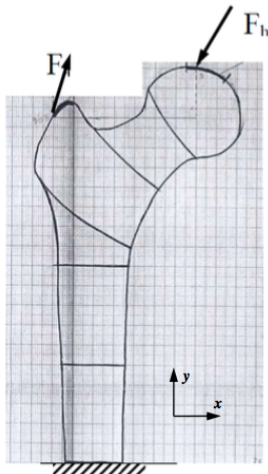


Figure 6: Proximal femur dimensions. Each square represents  $5\text{mm}^2$ .

The thickness of the remaining parts was set to 40 mm. From the analysis of pelvic radiography of patients who underwent successful hip resurfacing<sup>12</sup> we concluded that hip resurfacing aims at: preserving femoral head size; placing the stem parallel to the tangent to the lower curve of the femoral neck; placing the stem under the main axis of the neck. In our model, the hip resurfacing prosthesis was placed in order to align the stem with the direction of the femoral neck, with an angle of  $125^\circ$  relative to the direction of the diaphysis.

The part prosthesis was given the correspondent material properties (*see* Figure 4).

The elastic modulus of the bone parts was obtained from the temperature field (*i.e.*, density). ABAQUS was given instructions to read the temperature from a separate file, which in turn is updated at each iteration. The densities and elastic moduli are related through equation 4. The density of the side plate was set as the one of cortical bone,  $1.74 \text{ g/cm}^3$ . Furthermore, our modelling was based on the assumption of complete bonding between the prosthesis and the bone, which in ABAQUS corresponds to a Tie type of interaction between all the parts.

The mesh was defined using the medial axis options, which provides straighter meshes. We used a quadrangular element shape and two different meshes, a simpler one and a more refined one.

The surfaces of load application were chosen according to the location of the insertion of the abductor muscles and the average region of interaction with the acetabulum.

The reporting of the energies was done with the mode *Unique Nodal*, in which they are obtained by interpolation through nodes instead of elements<sup>13</sup>.

## 5.2 Huiskes Model Implementation

### 5.2.1 Bone Remodeling Parameters

The input to the Huiskes Model is a single scalar value  $U_a$  which is directly obtained from the results provided by ABAQUS after each iteration. The step value (*i.e.*,  $\Delta t \times B$ ) may be adjusted through the protocol.

---

<sup>12</sup>The images were obtained from the Orthopaedic Surgery department at Hospital de Santa Maria, Lisbon, Portugal.

<sup>13</sup>This procedure avoids the *chess* effect



Figure 7: Hip resurfacing dimensions and placement.

The reference value  $k$  is the average strain density, or the starting density corresponding to the middle of the plateau. It is not a standard value and should be adapted to each particular situation. We started by looking at the strain energies obtained with one iteration and choose a value for  $k$  that is within the range of energies of all the elements and from then one studied other values. The choice of the  $k = 0.0025J/g$  is justified with the results obtained in Section 6.1.2.

Starting with the consideration of young bone with a great sensitivity to mechanical stimuli, we made several trials with  $s$  equal to 0% (*i.e.*, not considering a steady plateau). Later on, we tested plateaus with  $s$  set to 10, 20 and 40% of  $k$ . We also tested several step values (*i.e.*,  $\Delta t \times B$ ). In order to optimize the computational performance without compromising the consistency of our results, we chose a value of 40.

### 5.2.2 Forward Euler Method

In order to implement the bone adaptation in an iterative routine, the Huiskes Model differential equation (equation 2) is discretized according to the forward Euler method, given by:

$$\frac{d\rho}{dt} = K \rightarrow \frac{\rho_{t+\Delta t} - \rho_t}{\Delta t} = K \rightarrow \rho_{t+\Delta t} = \rho_t + \Delta t \times K \quad (8)$$

Combining equations 2 and 8, the discretized Huiskes Model becomes:

$$\rho_{t+\Delta t} = \begin{cases} \rho_t + \Delta t \times B \left( \frac{U_a}{\rho_t} - k(1-s) \right), & \text{if } \frac{U_a}{\rho_t} < k(1-s) \\ \rho_t, & \text{otherwise} \\ \rho_t + \Delta t \times B \left( \frac{U_a}{\rho_t} - k(1+s) \right), & \text{if } \frac{U_a}{\rho_t} > k(1+s) \end{cases} \quad (9)$$

in which  $\Delta t \times B$  is the *step*. Since we are considering multiple loads (*i.e.*, walking and stair climbing) for the same elements, the strain energy  $U$  has been replaced by the average strain energy  $U_a$ , given by:

$$\frac{U_a}{\rho} = \frac{1}{n} \sum_{i=1}^n \frac{U_i}{\rho} \quad (10)$$

For  $s = 0$  and  $k = 0$ , the  $i^{th}$  iteration computes the density  $\rho_i$  as

$$\rho_i = \rho_{i-1} + step \times \left( \frac{U_a}{\rho_{i-1}} \right) \quad (11)$$

### 5.2.3 Runge-Kutta Method

In order to improve the computational efficiency we decided to implement the fourth order Runge-Kutta method in alternative to the Forward Euler Method [14]. In a single step, this method reaches a more exact solution than the Forward Euler Method. We confirmed experimentally that we can use larger steps with this method and therefore reach the same solutions with significantly less iterations.

The differential equation we are trying to solve is the derivative of the density  $\rho$  with respect to time  $t$ , given by equation 2. Since  $d\rho/dt$  itself is a function of  $\rho$  but not of  $t$ , the fourth order formula simplifies to:

$$\begin{aligned} k_1 &= h \times f(\rho_n) \\ k_2 &= h \times f(\rho_n + \frac{1}{2}k_1) \\ k_3 &= h \times f(\rho_n + \frac{1}{2}k_2) \\ k_4 &= h \times f(\rho_n + k_3) \end{aligned} \quad (12)$$

$$\rho_{n+1} = \rho_n + h \times \left( \frac{1}{6}k_1 + \frac{1}{3}k_2 + \frac{1}{3}k_3 + \frac{1}{6}k_4 \right) \quad (13)$$

in which  $h$  is the step. In the case no plateau is considered,  $f(\rho_n)$  is given by:

$$f(\rho_n) = B \left( \frac{U_a}{\rho} - k \right) \quad (14)$$

### 5.2.4 MatLab

We applied a MATLAB routine to implement the bone remodelling equations.

The density gradient field is initialized as unitary and uniform. In each iteration of the method (*see* Sections 5.2.2 and 5.2.3), MATLAB updates the densities node by node. The two load cases are then run on the new density gradient field. With the results generated by the ABAQUS analysis, and reported through a PYTHON file, the average of the energies obtained for both loads is computed for all the nodes. The density of each one is updated according to equation 9. The densities are constrained to the interval  $0-1.74 \text{ g/cm}^3$ .

The full MATLAB code is provided in Appendix B.

## 6 Results and Discussion

The results presented in this section depict the density gradient distribution over the proximal femur, according to the color scale shown in Figure 8, in  $\text{g/cm}^3$ .

### 6.1 Normal Bone

#### 6.1.1 Changing Load Distribution

The load distribution across the surface was initially considered to be quadratic. However, the results were slightly different from the ones expected. Namely, there was a region of high density

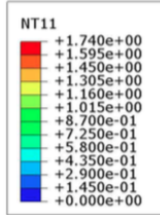
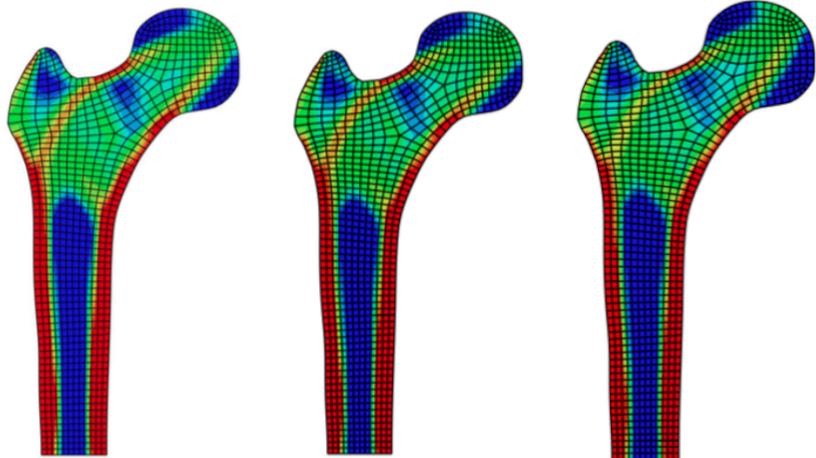


Figure 8: Color scale for density gradient in  $g/cm^3$  units.

connecting the lateral outer diaphysis to the superior neck from inside the bone, parallel to the high density connection between the medial outer diaphysis and the inferior face of the neck.

In a first attempt to correct this issue, we tested other types of load distributions - linear and uniform - across the surface. However, the results were identical to the ones obtained with the quadratic option (*see Figure 9*). For simplicity, we decided to stick to the uniform loads throughout the remaining modelling.

The next step was to reduce the surface of load application on the femoral head. With a reduction of the surface of load application on the femoral head, we obtained results that reproduce the ones in the literature (*see Figure 9*[15]. Namely, there was an increase of the angle of the high density border line in the inferior portion of the femoral head.



(a) Quadratic load distribution with larger surface. (b) Uniform load distribution with larger surface. (c) Uniform load distribution with smaller surface.

Figure 9: Bone remodeling results obtained for  $k = 0.0025J/g$ .

### 6.1.2 Changing Parameter $k$

For the initial assessment of  $k$ , the convergence criterion used to control the number of iterations was defined as the average of the density variation of all the elements between two consecutive iterations being less than 0.005. Regardless of this criterion, there is a maximum number of allowed iterations of 30, which with Runge-Kutta method allow a density variation of an order of 0.001 by the thirtieth iteration.

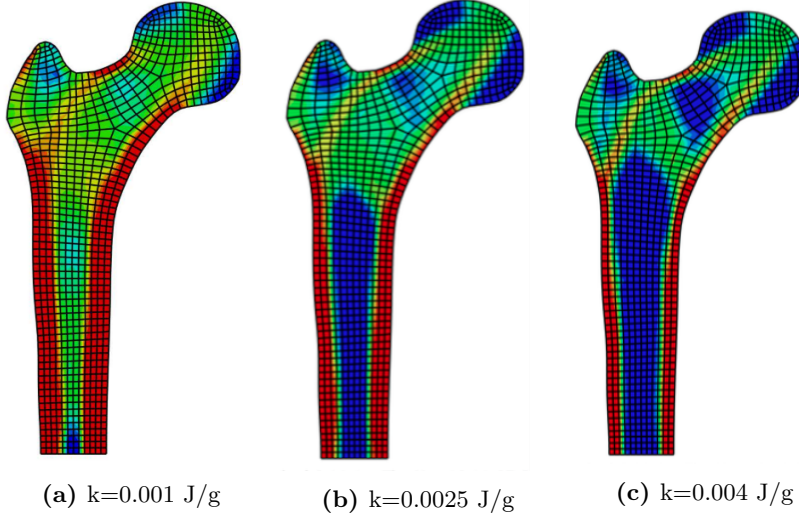


Figure 10: Bone remodeling with several values of  $k$ , for a 1014 node mesh and a step value of 40. See the remaining results for  $k$  value in appendix B.

With the reference value  $k$  set to 0.001 J/g, there was not enough loss of density in interior of the diaphysis and also in the epiphysis. For  $k$  equal to 0.0025 J/g (one of the values found in literature), we obtained a density gradient distribution that can be correlated with the bone type: very high densities are found in the lateral sides of the diaphysis, corresponding to cortical bone, and extremely low densities in its interior, forming a medullary cavity; Most of the epiphysis acquires the density of trabecular bone.

Within the later region, the anatomical groups of trabecula can be identified: in the femoral head, higher density near the regions of load application, corresponding to the principal compressive group; the densities are also greater in the regions of the great trochanter group (next to the surface of muscle load application) and the secondary compressive and tensile groups. There is high density in the epiphyseal line, under the greater trochanter, in the more distal region of the principal tensile group, even though its component in the femoral head does not appear in these results. The triangular region of low density in the middle of the femoral neck is the Ward Triangle, depicted in Figure 11. It is not located exactly as expected, probably due to the over simplification of the loading profile in the femoral head used in this model. Besides overall resembling the pattern shown in Figure 11, this density distribution is also in agreement with the one reported by Hernandez *et al.*

For a value of  $k$  of 0.004 J/g, the medullary cavity is greater than expected, taking over a portion of the epiphysis. Also, the low density triangle in the neck is more pronounced and more roughly shaped than expected (see Figure 11). These results appear to be less physiological than the ones obtained with 0.0025 J/g.

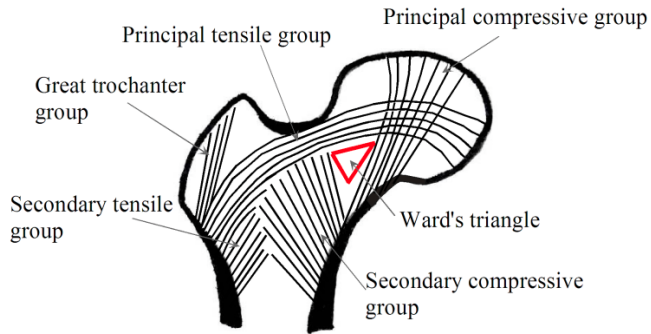


Figure 11: Trabecular pattern of proximal femur.

In order to reassure the choice of the value of  $k$ , the mesh was refined from 1014 to 7951 nodes. With the improved mesh, the values of  $k$  of 0.0025 and 0.003 J/g were tested. Since both of them yielded good results, we chose an intermediate value for the remaining analyses - 0.00275 J/g. With  $k=0.003$  J/g, the Ward Triangle is slightly extended, crossing most of the femoral neck. This might simulate a situation of initial bone loss, which is physiologically expected in aged bone. Loss of density in this area may be related to the high incidence of femoral neck fractures.

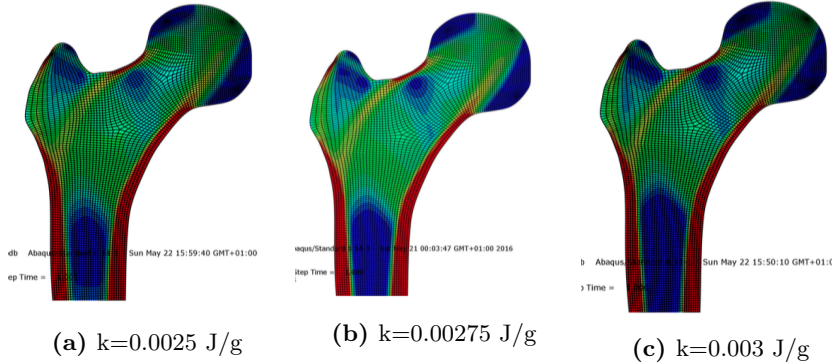


Figure 12: Bone remodeling with several values of  $k$ , for a 7951 node mesh and a step value of 40.

We faced an issue when running the iterative method with the refined mesh while maintaining the previous convergence criteria. The results obtained were not the same, the density lines having become too pronounced. Most likely, the model advanced more than needed, indicating that the convergence criterion that we used was not adequate. In order to prevent this issue in subsequent trials, we did an analysis of the results at every five iterations, both for the refined mesh and for the model with the implant.

### 6.1.3 Changing Parameter s

The first plateau considered was chosen so that it would include the two values of  $k$  that provided good results (0.0025 and 0.003 J/g, *see* Section 6.1.2). Furthermore, plateaus with half width  $s$  equal to 20 and 40 % were analysed.

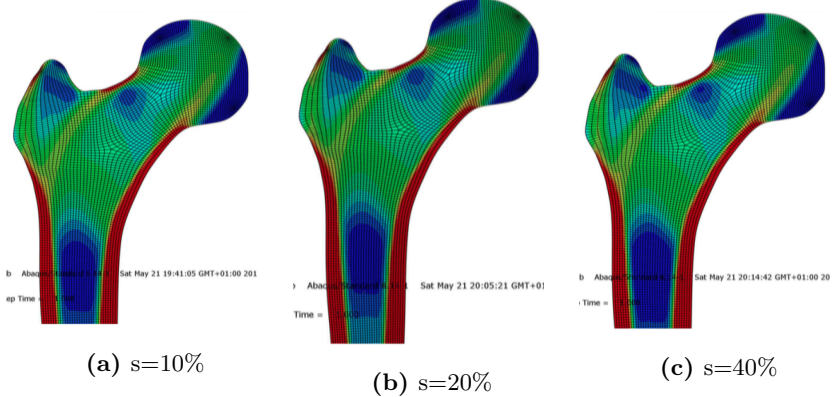


Figure 13: Bone remodeling for different values of  $s$ , with  $k = 0.00275\text{J/g}$ .

The results shown in Figure 13 were obtained with 13 iterations and a step of 40 (the model was also run for 25 iterations but no significant differences were detected). All the values of  $s$  yielded very similar results.

## 6.2 Hip Resurfacing

In this part of the modelling the amount of diaphysis considered was reduced (distally), since its consideration does not impact the results in the most proximal portion, which is the area of main concern in hip resurfacing.

### 6.2.1 Full Co-Cr vs Iso-Elastic Stem

Hip resurfacing was tested with both a Co-Cr alloy and a Iso-Elastic stem. In a practical application, a stem made of a titanium alloy would be a convenient way of approaching iso-elasticity (*see* Section 2.2.3 to recall the drawbacks of mixing two metals in a single prosthesis piece).

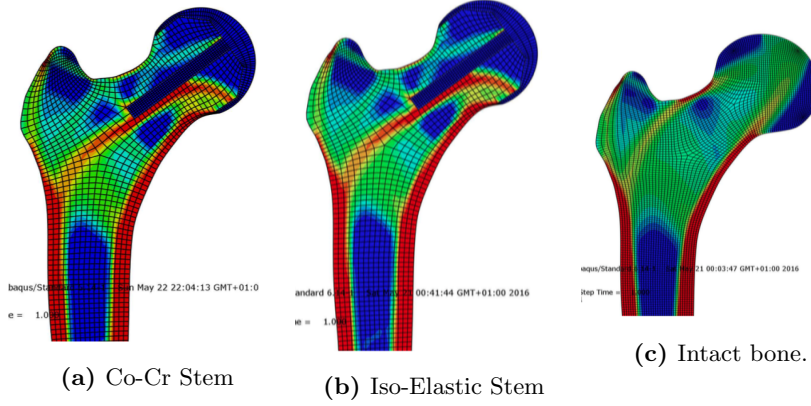


Figure 14: Bone remodeling with Co-Cr hip resurfacing and with different stem materials, and also with intact bone,  $k=0.00275 \text{ J/g}$ .

## 6.2.2 Changing Stem Size

Initially, we considered the stem size of the original model (50 mm). Afterwards, the lengths 75 mm and 25 mm were tested as well.

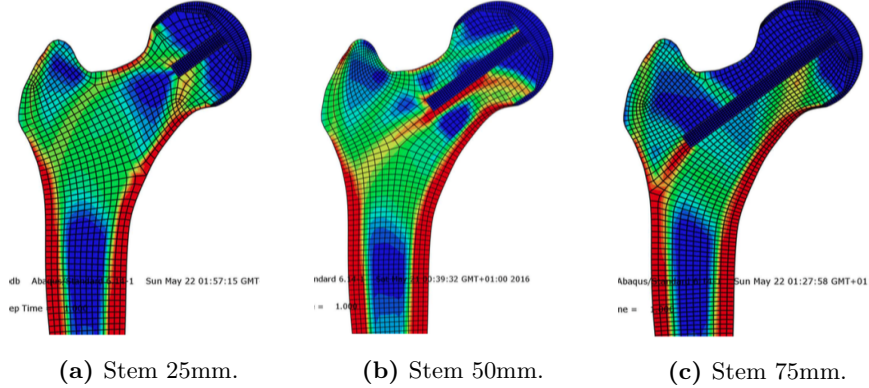


Figure 15: Bone remodeling with hip resurfacing with different stem sizes.

From Figure 15 it appears that the longest stem leads to significant density loss in the region above it, which ultimately may compromise its own support. With medium to long stems, part of force passes under the stem and another part above it (*i.e.*, although force is applied on the superior part of the head, there is force passing through the inferior part of the hip resurfacing cup). As initially predicted, reinforcement of the bone distally to the stem end can be observed with all stem sizes.

## 7 Conclusions

From the intact bone remodelling model we were able to select 0.00275 J/g as the appropriate value of the parameter  $k$  for the Huiskes Model implementation. We also concluded that the introduction of the reference values of  $s$  9, 20 and 40 % (*i.e.* plateaus of several widths) does not

lead to any improvement of the results. The fourth order Runge-Kutta method was successfully implemented; we note that the same result was obtained either by doubling the step size or doubling the iterations. The convergence criterion would have been more adequate if we had considered the average density variation in a given volume instead of a given node.

Although bone modelling with ABAQUS does not allow the simulation of the anisotropic behavior of bone, the density distribution obtained nicely reproduced the anatomical features of the proximal femur. The differences obtained relative to the theoretical anatomical models might have been reduced if we considered a more detailed loading pattern. Namely, the weighting of the energies could be altered in order to reproduce a more realistic proportion between the gait and the stair climbing movements. Including more loading cases and considering several application surfaces, could also improve the approximation to the cyclic nature of the hip joint movements, since both the loads and the points of application change constantly through time.

From this analysis we can make some predictions regarding the density alterations due to hip resurfacing. Longest stem leads to greatest bone resorption, which may compromise viability of bone. Although the bone might become less fragile with the use of shorter stems, the results regarding the stability of the prosthesis should also be evaluated. In the model used for this study, however, the study of stability is not possible, since we use a tie type of interaction. Furthermore, we note that the use of a tie interaction does not reproduce a non cemented prosthesis. In order to improve this analysis we could have used a contact type of interaction. Also, since we do not include a damage model, the results obtained assume that the bone would have withstood any loads that were applied during the analysis. The bone could have been damaged under high loads, leading to micro fractures that in a real situation would have compromised the bone remodelling process.

Another limitation of this approach is the assumption that the initial density distribution does not influence the final result. Due to need of reformulating the mesh when implementing the model with the prosthesis, we were not able to use the final densities obtained in the intact model as the initial densities in the hip resurfacing model. Also, the refined mesh was not ideal: namely, in the case of the smaller stem, there is an interruption of the internal wall which indicates a defect of the mesh. Further investigation should be done regarding the impact of variations in cup size, cup shape and stem angle.

## References

1. Park, J. & Lakes, R. *Biomaterials: An Introduction* (ed Springer) (2007).
2. Eurico, J. *Bone - Lecture Slides* (FMUL, 2015).
3. Folgado, J. & Fernandes, P. *Bone Tissue Mechanics* (IST, 2015).
4. Hall, S. *Basic Biomechanics* 6th ed. (ed McGraw-Hill) (2011).
5. Christian Pfirrmann and Christine Chung. Greater Tochanter of the Hip: Attachment of the Abductor Mechanism and a Complex of Three Bursae. *Radiology* (1998).
6. Monteiro, J. *Biomateriais em Cirurgia Ortopédica* (FMUL, 2016).
7. F Netter. *Atlas of Human Anatomy* 5th ed. (Elsevier - Health Sciences Division, 2010).
8. Williams, D. *Essential Biomaterials Science* (ed Press, C. U.) (2014).
9. R Huiskes and H Weinans. Adaptative Bone-Remodeling Theory Applied to Prosthetic-Design Analysis. *J. Biomechanics* **20** (1987).

10. Martinho, M., Manso, A. & Monteiro, S. *Análise por método de elementos finitos de um problema de elasticidade plana – modelo de fémur em regime de carga associado ao movimento de subir escadas* (IST, 2015).
11. Reddy, N. *An Introduction to the Finite Element Method* 3rd ed. (ed McGrawHill) (2006).
12. W Lai and D Rubin and E Krempl. *Introduction to Continuum Mechanics* 3rd ed. (Butterworth-Heinemann, 1999).
13. Jacobs, C., Levenston, M., Simo, J., Beaupré, G. & Carter, D. Numerical instabilities in bone remodeling simulations: The advantage of a node-based finite element approach. *Journal of Biomechanics* **28** (1995).
14. Zeltkevic, M. *Runge-Kutta Methods - Introduction to Computer Methods Class Notes* (IST, 1998).
15. Christopher J Hernandez and Gary S Beaupré and Dennis R Carter. A model of mechanobiologic and metabolic influences on bone adaptation. *JRRD* **37** (2000).

## Appendices

### Appendix A

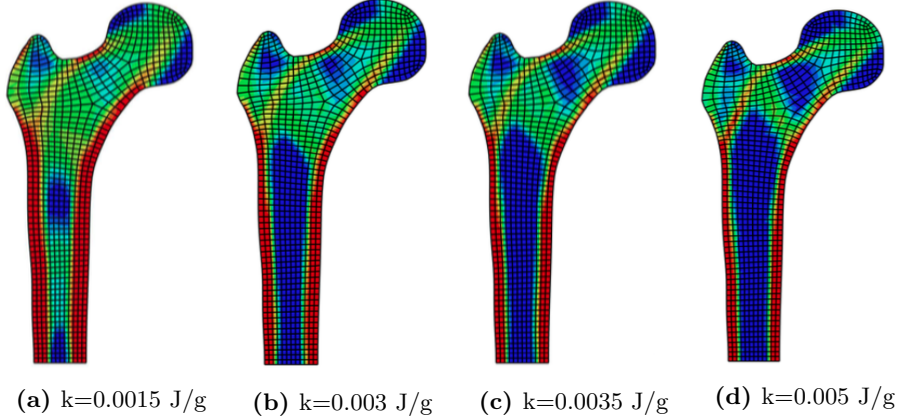


Figure 16: Bone remodeling with several values of  $k$ , for a 1014 node mesh and a step value of 40.

### Appendix B

```
% Configuracoes
disp('Configura do modelo:');
nodes=input('nodes= ');
k=input('k= ');
disp('Deseja usar modelo com plateau? sim =1 nao=0');
plateau=input('= ');
if(plateau==1)
    s=input('s= ');
end
step=input('step= ');
niter=input('nr iteracoes= ');
cconv=input(' criterio de convergencia = ');
B=1;
n=1000;
%
% inicializaaao das densidades a 1
dens=1*ones(1,nodes);
densold=zeros(size(dens));
% Ciclo para o calculo iterativo
for iter=1:niter
    % Avisa qual a itera do processo
    disp(' ');
    disp(sprintf('Iteracao %g',iter));
    %
    % Escreve as densidades para um ficheiro que o abaqus ir utilizar
    fich=fopen('dense.dat','w');
    for i=1:nodes
        fprintf(fich,'femur-1-1.%d, %f\r\n',i,dens(i));
    end;
    fclose(fich);
```

```

% -----Modelo andar-----
%
% Correr Abaqus
dos('abaqus job=job_andar inter');
%
%
% Guardar a cada 5 iteraes os resultados
if(rem(iter,5)==0)
fname=sprintf('iteracao_%d.odb',iter);
copyfile('job_andar.odb',fname);
end
%
% Retirar a Strain Energy calculada pelo Abaqus
dos('abaqus viewer noGUI=extract_andar.py');
%
% Obter as Strain Energies do ficheiro txt
fich = fopen('sener_andar.txt');
while 1
    tline = fgetl(fich);
    if feof(fich),break,end
    if strcmp(tline,'-----') == 1
        dados1 = (fscanf(fich,'%g %g',[2 inf]))';
    end
end
fclose(fich);
% Guardar as energias num vetor
ener1=dados1(1:nodes,2);
%
% -----Modelo correr-----
%
% Correr Abaqus
dos('abaqus job=job_correr inter');
%
%
% Retirar a Strain Energy calculada pelo Abaqus
dos('abaqus viewer noGUI=extract_correr.py');
%
% Obter as Strain Energies do ficheiro txt
fich = fopen('sener_correr.txt');
while 1
    tline = fgetl(fich);
    if feof(fich),break,end
    if strcmp(tline,'-----') == 1
        dados2 = (fscanf(fich,'%g %g',[2 inf]))';
    end
end
fclose(fich);
% Guardar as energias num vetor
ener2=dados2(1:nodes,2);
%
%
%Runge-Kutta 4 Ordem
%-----Modelo com s-----
if(plateau==1)
for i=1:nodes
    if( (ener1(i)+ener2(i))/dens(i) > k*(1+s))
        k_1 = B*((ener1(i)+ener2(i))/(2*dens(i))-k*(1+s));
        k_2 = B*((ener1(i)+ener2(i)) / (2*(dens(i)+0.5*k_1)) -k*(1+s));
        k_3 = B*((ener1(i)+ener2(i)) / (2*(dens(i)+0.5*k_2)) -k*(1+s));
        k_4 = B*((ener1(i)+ener2(i)) / (2*(dens(i)+k_3)) -k*(1+s));
    elseif( (ener1(i)+ener2(i))/dens(i) < k*(1-s))
        k_1 = B*((ener1(i)+ener2(i))/(2*dens(i))-k*(1-s));
    end
end

```

```

k_2 = B*( (ener1(i)+ener2(i)) / (2*(dens(i)+0.5*k_1)) -k*(1-s));
k_3 = B*( (ener1(i)+ener2(i)) / (2*(dens(i)+0.5*k_2)) -k*(1-s));
k_4 = B*( (ener1(i)+ener2(i)) / (2*(dens(i)+k_3)) -k*(1-s));
else
    k_1 = 0;
    k_2 = 0;
    k_3 = 0;
    k_4 = 0;
end
%Guarda densidade antiga
densold(i)=dens(i);
%Calculo da nova densidade
dens(i) = dens(i) + (1/6)*(k_1+2*k_2+2*k_3+k_4)*step;
%Limites das densidades
if dens(i) > 1.74
    dens(i)=1.74;
end;
if dens(i) < 0.01
    dens(i)=0.01;
end;
end;
%-----Modelo sem s-----
elseif(plateu==0)
for i=1:nodes
    k_1 = B*((ener1(i)+ener2(i))/(2*dens(i))-k);
    k_2 = B*( (ener1(i)+ener2(i)) / (2*(dens(i)+0.5*k_1)) -k);
    k_3 = B*( (ener1(i)+ener2(i)) / (2*(dens(i)+0.5*k_2)) -k);
    k_4 = B*( (ener1(i)+ener2(i)) / (2*(dens(i)+k_3)) -k);
    %Guarda densidade antiga
    densold(i)=dens(i);
    %Calculo da nova densidade
    dens(i) = dens(i) + (1/6)*(k_1+2*k_2+2*k_3+k_4)*step;
    %Limites das densidades
    if dens(i) > 1.74
        dens(i)=1.74;
    end;
    if dens(i) < 0.01
        dens(i)=0.01;
    end;
end;
end

%Calculo da media do modulo da varia das densidades
sum=0;
for i=1:nodes
    sum = sum + abs(dens(i)-densold(i));
end
%mostra a mdia da variacao das densidades
disp(sum/nodes);
%criterio de convergencia
if(sum < nodes*cconv)
    if(iter==n)
        break;
    end
    n=1+iter;
end

end

```